# Vertical vibrations of composite bridge/track structure/high-speed train systems. Part 1: Series-of-types of steel-concrete bridges

## M. PODWORNA[1] and M. KLASZTORNY[2*]

[1] Institute of Civil Engineering, Wroclaw University of Technology, 27 Wyspianskiego St., 50-370 Wroclaw, Poland
[2] Department of Mechanics and Applied Computer Science, Military University of Technology, 2 Kaliskiego St., 00-908 Warsaw, Poland

**Abstract.** A new series-of-types of single-span simply-supported railway composite (steel-concrete) bridges, with a symmetric platform, has been designed according to the Polish bridge standards. The designed bridges/viaducts are located on the main railways of the classification coefficient $k = +2$. A ballasted track structure adapted to high operating speeds has also been designed. The ultimate limit states and the limit states corresponding to the bridges undertaken are collected and discussed. The bridges have been designed in accordance with contemporary art engineering, with geometric and material optimization, avoiding overdesign. A new methodology of numerical modelling and simulation of dynamic processes in composite bridge/ballasted track structure/high speed train systems, developed in Part 2 and Part 3, has been applied and implemented in a problem-oriented computer programme. A new approach to predicting forced resonances in those systems is formulated and tested numerically. It has been proved that in the case of typical structural solutions of bridges and ballasted track structures, it is necessary to introduce certain limitations for operating speeds of trains.

**Key words:** composite steel-concrete bridge, ballasted track structure, high-speed train, design, FE modelling, simulation, forced resonances, numerical analysis.

## 1. Introduction

Composite (steel-concrete) bridges loaded by high-speed trains need to be designed or modernized to ensure the traffic safety condition (TSC) and the passenger comfort condition (PCC), among the others (EN 1990 Eurocode: Basis of structural design. Annex A2: Application for bridges, 2004). Too large vertical accelerations of the bridge platform may cause ballast destabilization in the track structure. This problem was investigated at ERRI to establish the safe limits (ERRI. D214/RP9, Part B, Rail bridges for speeds >200 km/h, Utrecht, The Netherlands, European Rail Research Institute, 1999), later incorporated in EN 1990 Eurocode: Basis of structural design. Annex A2: Application for bridges, 2004, EN 1991-2, Eurocode 1: Actions on structures. Part 2: General actions – traffic loads on bridges, 2003, in which dynamics of railway bridges under high-speed trains is standardized. To date, each railway bridge has been designed singly.

The study presents a series-of-types of single-span simply-supported railway composite (steel-concrete) bridges, with a symmetric platform, as well as a ballasted track structure adapted for high-speed trains, both designed according to Polish standards PN-85/S-10030. Bridge objects. Loads, PN-82/S-10052. Bridge objects. Steel structures. Design, PN-91/S-10042. Bridge objects. Concrete, reinforced concrete and pre-stressed concrete structures. Design. A new methodology of numerical modelling and simulation of dynamic processes in a composite bridge/ballasted track structure/high speed train (BTT) system, developed by Podworna and Klasztorny [1], has been applied. Computer algorithms of FE modelling and simulation have been programmed in Del-

phi [2]. Both, static and dynamic numerical investigations of the bridges forming the series-of-types have been carried out. It has been proved that in the case of typical structural solutions of bridges and ballasted track structures, it is necessary to introduce certain limitations for service speeds of trains. Extended literature review results in dynamics of railway bridges loaded by high-speed trains is presented in [1].

## 2. Series-of-types of railway bridges

The study develops design of a series-of-types of composite (steel-concrete) railway beam bridges. There is developed a series-of-types composed of five objects of codes and basic geometric parameters compared in Table 1. Theoretical span lengths 15, 18, 21, 24, and 27 m are commonly used in design of the bridges undertaken.

Table 1
Codes and basic geometric parameters of objects forming SCB series-of-types

| Bridge code | SCB-15 | SCB-18 | SCB-21 | SCB-24 | SCB-27 |
|---|---|---|---|---|---|
| Theoretical span length $L$ [m] | 15.00 | 18.00 | 21.00 | 24.00 | 27.00 |
| Total span length [m] | 15.80 | 18.80 | 21.80 | 24.80 | 27.80 |
| Structural height [m] | 1.82 | 1.97 | 2.12 | 2.27 | 2.42 |

The SCB series-of-types of railway bridges was designed according to standards PN-85/S-10030, PN-82/S-10052, PN-91/S-10042, under the following assumptions:

- bridges/viaducts are located on the main railways of classification coefficient k=+2,
- axis of an unloaded railway track is rectilinear horizontal,

---

- track gauge is adapted for high-speed trains and is equal to 5.10 m,
- bridges are composite (steel-concrete) and have separate spans for each track,
- bridges are single-track and simply supported,
- a number of railway tracks is optional.

A reference object is a modernized composite viaduct described in the technical documentation "Modernization of composite viaduct KNI 140070 situated in km. 200.794 of railway No. 4 – E 65 Grodzisk Mazowiecki – Zawiercie, Construction project, Polish Railways Office, Warsaw, 2008". Construction of the bridges and the track is illustrated with a case of SCB-15 bridge in Figs. 1–4. There are significant differences between the objects of SCB series-of-types and the reference object. The technical data of SCB series-of-types objects are as follows:

- the superstructure is composed of four steel I-beams and a RC plate platform,
- main steel beams are 770–1370 mm high, they are produced of S235W steel, their lower chords are reinforced with one overlay 0.6 $L$ long,
- the main beams are reinforced vertically and horizontally in pairs with L100×100×10 angles using welding,
- in the supporting areas of the main beams, there are 50 mm thick bearing plates welded to the lower chords of the main beams and three vertical ribs welded to the I-beams,
- 10 mm thick vertical ribs, welded to the I-beam webs, are positioned at intervals of 1500 mm,
- discrete connection of the main steel beams with the RC platform plate is executed with the use of steel anchors of dimensions $\varphi 12$ mm, $l = 170$ mm, welded to the upper chords of the beams and anchored in the RC platform plate; the anchors are spaced properly in both the longitudinal and transverse direction to protect practically non-deformable connection,
- an RC platform plate is 250 mm thick, produced of B35 concrete and reinforced with AII/18G2-B steel,

- levelling concrete layer of 0–40 mm thickness is characterized by a 2% two-sided transverse slope,
- concrete kerbs of the platform plate are 250 mm high, they are produced of B17 concrete and reinforced structurally; there are applied a technological stop at the level of the upper surface of the RC platform plate and 1 cm wide vertical dilatations at intervals of 1.50 m,
- RC bridgehead foundations are used,
- approach slabs are supported with elastomeric bearings and produced of B35 concrete, reinforced with AII/18G2-B steel; their dimensions are 5.00 m – total length, 4.00 m – width, 20 cm – thickness, 2% two-sided transverse slope,
- in the transient zones, there is applied 150 kg/m$^3$ cement-stabilized soil,
- the track structure is composed of: continuously welded S60 main rails, S60 side rails of length covering the bridge span and the approach slabs, B320 U60, B320 U60-U PC sleepers, first class crushed stone ballast to the depth of 35 cm under sleepers in the track axis, Vossloh 300-1fasteners of the main rails, SB3 fasteners of the side rails,
- there is applied Elastomatic TF isolation which is resistant to direct action of the ballast that eliminates application of a protective concrete layer,
- there is applied a one-side service sidewalk (from the outer side),
- there are applied movable bearings of RESTON type, from the train entrance side, with a possibility of longitudinal displacement under each main beam; bearings under the outer beams have also transverse displacement available,
- there are applied unmovable bearings of RESTON type, from the side opposite to the train entrance side; bearings under the outer beams have also transverse displacement available.

Approach slabs are designed to minimize the threshold effect, eliminate a jump in subsidence of the ground in the area of the bridgehead, increase durability of the track in the bridgehead area.
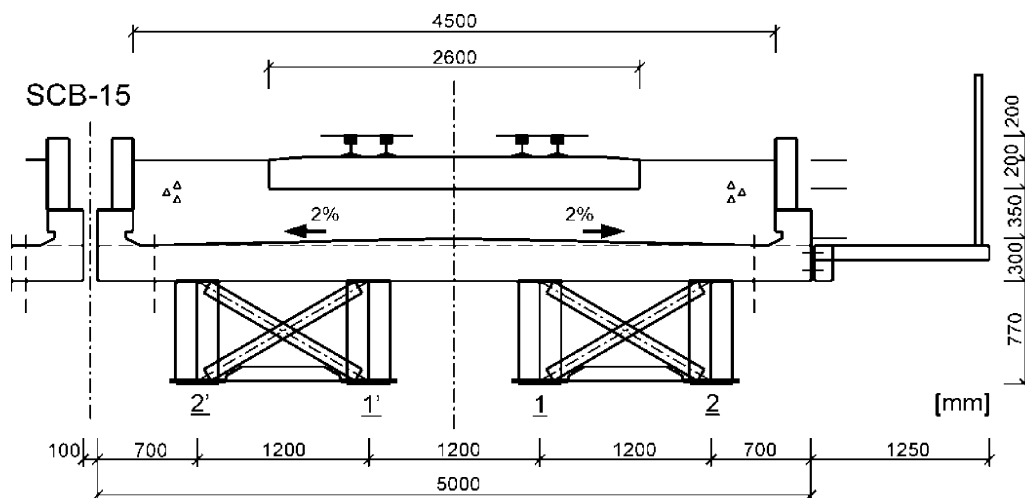


Fig. 1. Cross-section of SCB-15 bridge at midspan

www.czasopisma.pan.pl  www.journals.pan.pl

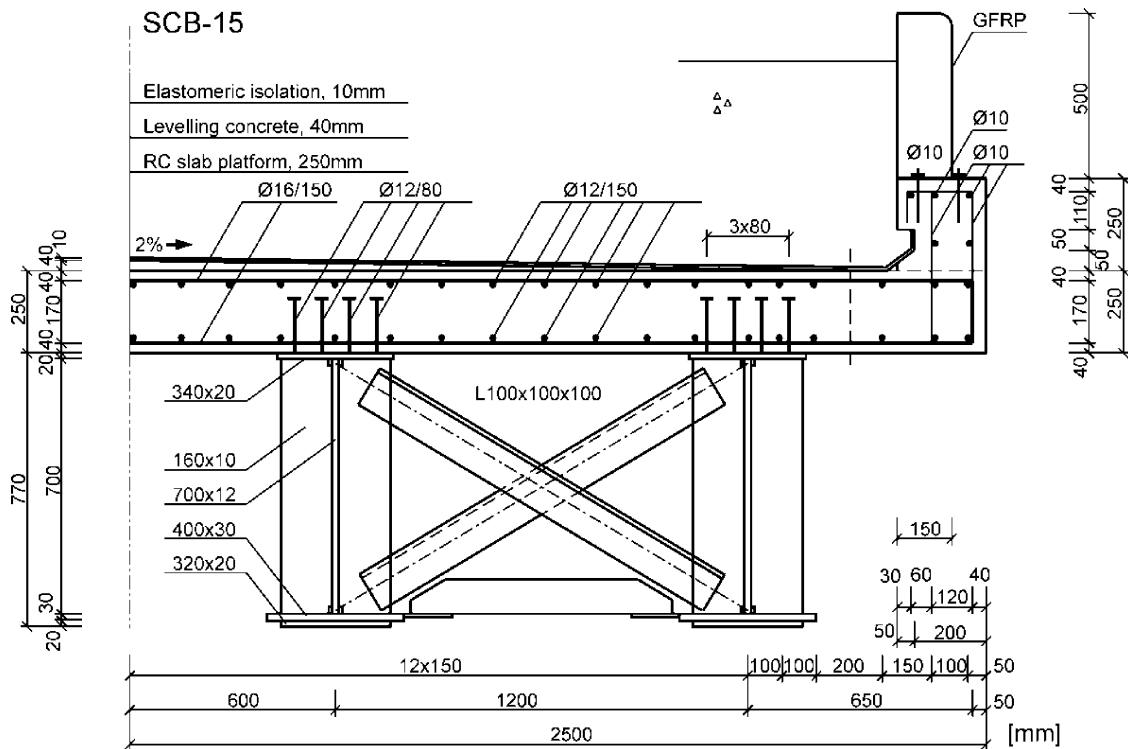*Vertical vibrations of composite bridge/track structure/high-speed train systems. Part 1*

Fig. 2. Cross-section of symmetric superstructure of SCB-15 bridge (main and structural reinforcement)
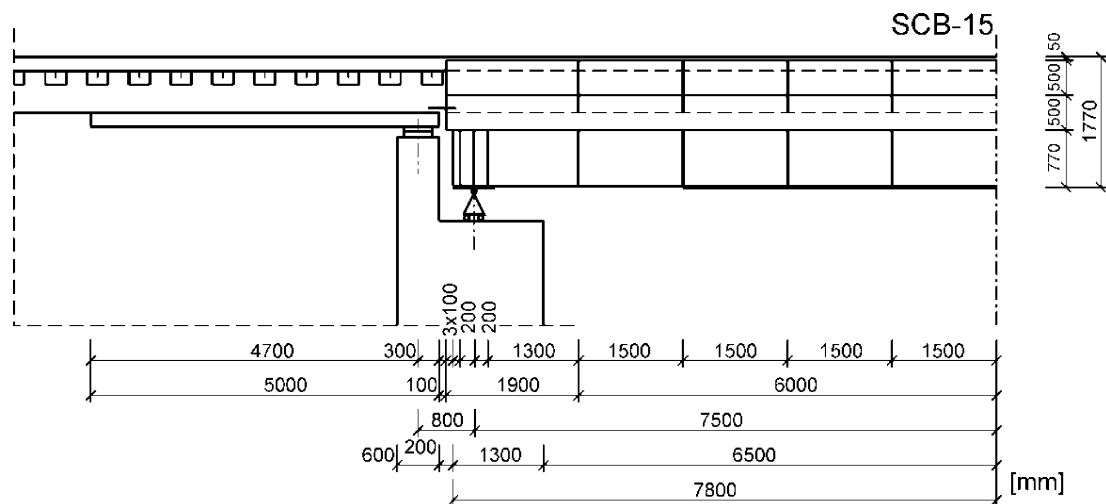


Fig. 3. Longitudinal section of symmetric bridge SCB-15 and of transient zone part

New structural properties of bridges forming the SCB series-of-types are as follows:

- full symmetric RC platform (minimization of flexural – torsional vibrations, elimination of vibration coupling of parallel neighbouring spans through the ballast),
- structurally reinforced low concrete kerbs of the platform plate, with application of technological stop and dilatations (elimination of a one-side RC wall inducing asymmetric vibrations of the span and increase in lateral and flexural – torsional vibrations),
- shell CFRP composite shields (resistant to vibrations) fixed to the kerbstones with steel anchors, with vertical dilatations 1 cm width and 1.49 m long, sustaining the ballast

between the kerbstones and decreasing the platform mass,
- four main steel I-beams joined in pairs, with the use of vertical and horizontal brackets, with no brackets between the beam pairs,
- bearings unmovable transversally under each inner beam (better transfer of the horizontal loads on the main beams),
- back walls of the bridgeheads with increased thickness in order to support the approach slabs with elastomeric bearings.

Figure 1 shows a cross-section in the span centre of bridge SCB-15. Cross-sections of bridges SCB-18, SCB-21, SCB-24, SCB-27 are analogous; only the web and lower chords of the main beams as well as the vertical brackets are subjected
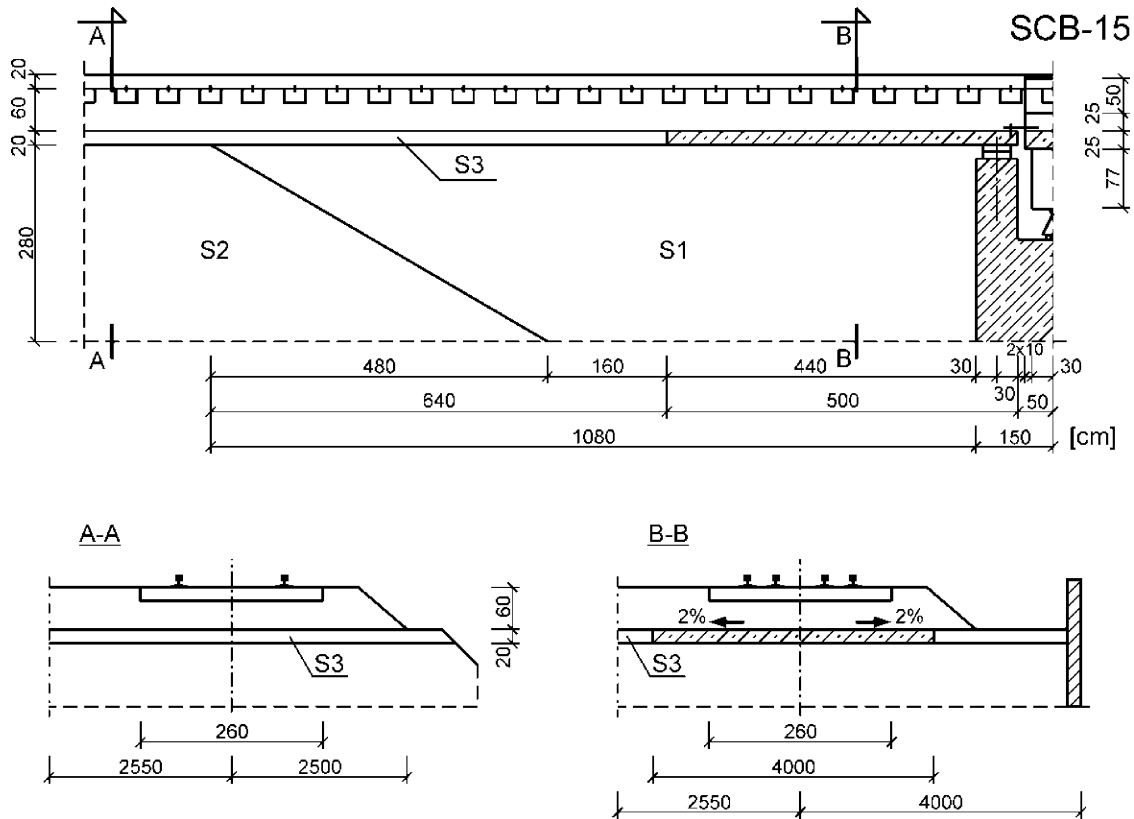
M. Podworna and M. Klasztorny



Fig. 4. Longitudinal section of transient zone and cross-sections of track outside this zone (A-A) and in approach slab zone (B-B)

to respective changes. Figure 2 presents a cross-section of a half of the SCB-15 bridge superstructure, including transverse main reinforcement and longitudinal structural reinforcement of the platform plate, longitudinal and transverse structural reinforcement of the kerbstones. The detailed geometry of the solution is provided.

Figure 3 demonstrates a longitudinal section of bridge SCB-15 and the initial part of the transient zone. One can see ribs stiffening webs of steel beams at 1500 mm intervals, support ribs located every 200 mm, a bearing plate 600 mm long, an overlay of a lower chord of the length of $0.6L = 9000$ mm, kerbstones with 1 cm dilatations every 1500 mm, CFRP composite protective walls with 1 cm dilatations every 1500 mm, an approach slab of the total length of 5000 mm. Figure 4 depicts the transient zone. One can see the S1 cement-stabilized soil zone, the S2 nonwovens reinforced embankment ground, the S3 sand–gravel mix layer under the ballast, the approach slab. There are shown a cross-section of the track outside the transient zone and in the approach slab zone.

Engineering calculations of bridges forming the SCB bridge series-of-types were conducted according to PN-85/S-10030, PN-82/S-10052, PN-91/S-10042 and [3]. The following construction technology of composite girders was adopted:

- assembly on the stiff scaffolding (composite superstructure operates only in phase II),
- no initial stresses incorporated in steel beams before their connection to a RC platform plate,

- concrete of the platform plate produced of a mixture of plastic consistency,
- concreting the platform plate section by section; a break between concreting the subsequent sections ≥ 8 hours,
- concrete curing in normal conditions during 28 days.

This technology is the best one from a point of view of static effort (under dead load) and dynamic effort (under live load) of the composite superstructure.

In the engineering calculations the following assumptions are adopted:

- the composite cross-section operates in a linear – elastic range,
- steel beams – concrete platform connection is non-deformable (linear distribution of longitudinal normal strains at bending),
- a composite cross-section is reduced to the equivalent steel cross-section,
- dimensioning for elastic ultimate limit states (stresses resulting from design loads not exceeding design strength),
- dimensioning for limit states (displacements/vibrations induced by characteristic loads not exceeding displacement limits),
- a transverse distribution of the loads corresponds to the rigid cross-member assumption,
- torsional stiffness of the composite superstructure is not considered (bracings connect main beams in pairs),
- ribs of the main I-beams meet the requirements set for stiff ribs.

www.czasopisma.pan.pl    PAN    www.journals.pan.pl

POLSKA AKADEMIA NAUK

*Vertical vibrations of composite bridge/track structure/high-speed train systems. Part 1*

Complete engineering calculations include [3]:

1. stresses induced by dead loads (with assembly technology taken into consideration),
2. stresses induced by vertical live loads (vertical moving load),
3. stresses induced by rheological effects (concrete creep and shrinkage with creep taken into consideration),
4. stresses induced by horizontal live loads (wind load, lateral impacts of moving trains),
5. stresses induced by thermal effects.

In the case of the basic system of loads (P), stresses of the 1, 2, 3 types are taken into account. In the case of the basic and additional systems of loads (PD), stresses of the 1, 2, 3, 4, 5 types are taken into account. In the case of the basic and exceptional systems of loads (PW), exceptional loads, e.g., train derail, are also taken into account. The least advantageous system (P, PD or PW) is accepted for the dimensioning.

Complete check-up of elastic ultimate limit states includes [3]:

1. check the composite girder load capacity (longitudinal normal strains, shear),
2. check the RC platform plate load capacity,
3. check the steel beams for fatigue,
4. check the steel beams – RC platform plate connection load capacity,
5. check the welded joints and other joints of bridge span elements,
6. check the compressed chords of the steel beams for lateral-torsional buckling (absent in the applied solution),
7. check the load capacity for local stability of I-beam webs,
8. check the position stability of bridge spans (overturning or sliding).

In the case of check-up 1, 2, 4, 5, 6, 7, there are the design stresses, dynamic coefficient and design strengths taken into account. In the case of check-up 3, there are the characteristic stresses, dynamic coefficient, fatigue coefficient $m_{zm}$ (PN-82/S-10052), design strengths taken into account. In the case of check-up 8, the characteristic loads (without dynamic coefficient) are taken into consideration.

Check-up of connection of the steel part with the concrete part includes (PN-82/S-10052):

- load capacity of connectors,
- load capacity of fixing to steel girders,
- load capacity of concrete around a connector.

Complete check-up of limit states includes [3]:

1. check the deflection of a composite girder under moving load,
2. check the horizontal stiffness of a bridge,
3. design of the negative structural deflection,
4. check the concrete crack limit state (initiation and opening of transverse cracks; absent in case of applied solution and construction technology),

5. check the fatigue limit state (durability protection of composite bridge),
6. check the limit state of comfort,
7. check limit states of rail traffic safety:
- vertical vibrations of a bridge,
- torsion of a platform,
- rotations at the ends of a platform,
- horizontal deformations of a platform.

The present work considers the following stresses in dimensioning of a composite cross-section of SCB series-of-types bridge objects:

- stresses induced by dead loads (with assembly technology taken into consideration),
- stresses induced by vertical live loads (vertical moving load),
- stresses induced by rheological effects (concrete creep and shrinkage with creep taken into consideration).

This is the basic load system (P). The ultimate limit state results in check-up of the composite girder load capacity (longitudinal normal stresses). The limit states include:

- check the deflection of a composite girder under moving load,
- check the fatigue limit state (durability protection of composite bridge),
- check the limit state of comfort,
- check the limit state of rail traffic safety in the scope of vertical vibrations of a bridge.

Material constants for the main materials (concrete, steel) are collected in Tables 2–4 [3].

Table 2
Material constants for B35 (C30/37) concrete of platform plate [3]

| characteristic compressive strength | $f_{ck}$ | 26.2 MPa |
|---|---|---|
| average value of compressive strength with 50% probability of exceeding | $f_{ck\,0.5} = f_{cm}$ | 34.2 MPa |
| average value of tensile strength with 5% probability of exceeding | $f_{ctk\,0.05}$ | 1.9 MPa |
| average value of tensile strength with 50% probability of exceeding | $f_{ctk\,0.5} = f_{ctm}$ | 2.7 MPa |
| elastic modulus ($0 < \sigma \leq 0.5 f_{ck}$) | $E_{cm}$ | 34.6 GPa |
| Poisson's ratio | $\nu$ | 0.167 |
| coefficient of thermal expansion | $\alpha$ | $1 \times 10^{-5}/K$ |

Table 3
Material constants for 18G2-B reinforcing steel (weldable) [3]

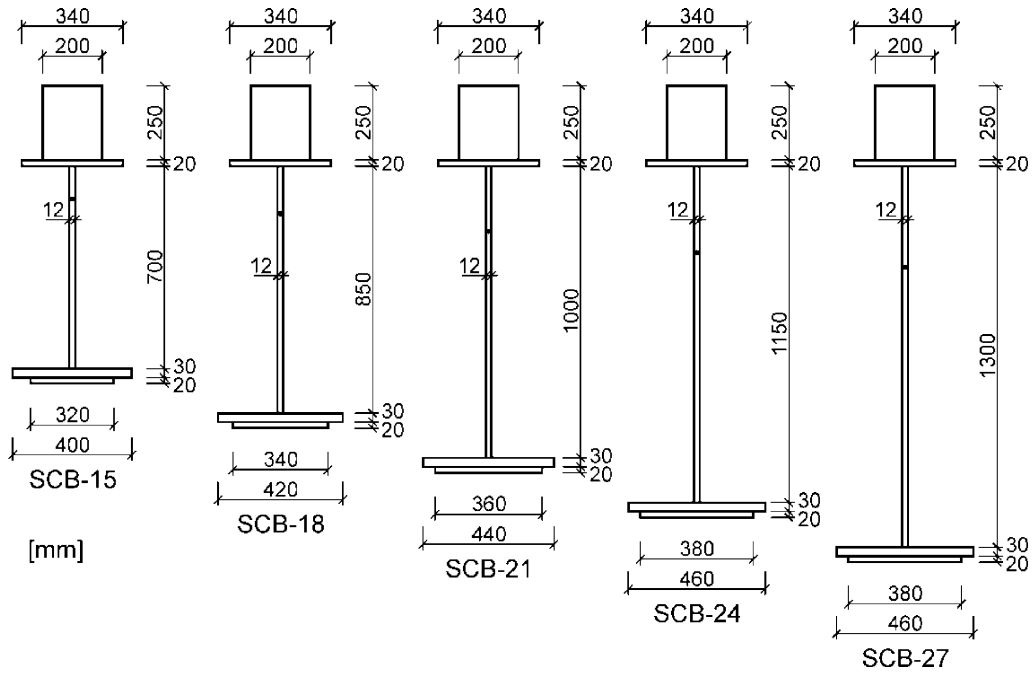| nominal diameter of rods | $d$ | 6–32 mm |
|---|---|---|
| characteristic yield stress | $f_{yk}$ | 355 MPa |
| characteristic strength | $f_{tk}$ | 480 MPa |
| elastic modulus | $E_s$ | 200 GPa |
| coefficient of thermal expansion | $\alpha$ | $1 \times 10^{-5}/K$ |

Fig. 5. Equivalent steel cross-sections corresponding to one beam in reference to SCB series-of-types bridges

Table 4

Material constants for S235W steel (weldable, increased resistance to atmospheric corrosion) [3]

| thickness of flats | $t$ | $\leq 40$ mm |
|---|---|---|
| elastic modulus | $E_a$ | 205 GPa |
| shear modulus | $G_a$ | 80 GPa |
| Poisson's ratio | $\nu_a$ | 0.30 |
| coefficient of thermal expansion | $\alpha_a$ | $1 \times 10^{-5}/K$ |
| characteristic yield stress | $f_{yk}$ | 235 MPa |
| characteristic strength | $f_{uk}$ | 360 MPa |

According to [3], the design compressive strength of concrete B35 at bending equals $f_{cd} = \dfrac{f_{ck}}{\gamma_c} = \dfrac{26.2}{1.5} = 17.5$ MPa, and the design shear strength amounts to $\tau_{Rd} = \dfrac{f_{ctk\,0.05}}{4\gamma_c} = \dfrac{1.9}{6} = 0.32$ MPa. The design strength of reinforcing steel 18G2-B is equal to $f_{sd} = \dfrac{f_{yk}m_s}{\gamma_s} = \dfrac{355 \times 1.0}{1.2} = 296$ MPa. Design strengths at tension, compression at bending, complex stress state for steel S235W equal $f_{ad} = \dfrac{f_{yk}}{1.05\gamma_a} = \dfrac{235}{1.05 \times 1.15} = 195$ MPa. The design shear strength of steel S235W is equal to $f_{adv} = 0.58f_{ad} = 0.58 \times 195 = 115$ MPa. The design pressure strength of flat surfaces for steel S235W equals $f_{add} = 1.25f_{ad} = 1.25 \times 195 = 245$ MPa. The effective cooperative width of the platform concrete plate is equal to spacing of the main steel beams, i.e., 1.20 m. The steel to concrete elastic modules ratio is equal to $\alpha = E_a/E_{cm} = 205/34.6 = 5.92$. The equivalent width of the concrete plate (for single steel beam) is equal to $b_s = \dfrac{1200}{5.92} = 203$ mm $\cong$ 200 mm.

The equivalent steel cross-sections corresponding to one beam in reference to the SCB series-of-types bridge objects are presented in Fig. 5. A dynamic coefficient for composite bridges is calculated from the formula [3]

$$\phi = \frac{1.44}{\sqrt{L} - 0.2} + 0.82. \qquad (1)$$

For the moving load class $k = +2$ one obtains the load class coefficient $\alpha_k = 1.21$ and the moving load coefficient $\gamma_f = 1.5$. Substitute distributed moving loads are equal to [3]:

- $p_{sk} = \alpha_k \times 80 = 1.21 \times 80 = 96.8$ kN/m – characteristic load without dynamic coefficient,
- $p_k = p_{sk}\phi$ – characteristic load with dynamic coefficient,
- $p_o = p_k\gamma_f$ – design load,
- $q_{sk} = \alpha_k \times 156 = 1.21 \times 156 = 189$ kN/m – characteristic load without dynamic coefficient,
- $q_k = q_{sk}\phi$ – characteristic load with dynamic coefficient,
- $q_o = q_k\gamma_f$ – design load.

The following bending moments were determined [kNm]:

- $M_{gk}(g_k)$ – bending moment induced by characteristic dead loads,
- $M_{usk}(p_{sk}q_{sk})$ – bending moment induced by characteristic moving loads without dynamic coefficient,
- $M_{uk}(p_kq_k)$ – bending moment induced by characteristic moving loads with dynamic coefficient,
- $M_{go}(g_o)$ – bending moment induced by design dead loads,
- $M_{uo}(p_oq_o)$ – bending moment induced by design moving loads with dynamic coefficient,
- $M_o = M_{go} + M_{uo}$ – design bending moment.

Tension stresses in the bottom fibres of the steel beams [MPa] were calculated from the following formulas [3]:

www.czasopisma.pan.pl    PAN    www.journals.pan.pl
POLSKA AKADEMIA NAUK

*Vertical vibrations of composite bridge/track structure/high-speed train systems. Part 1*

- $\sigma_{ak} = 0.001(M_{uk} + M_{gk})/W_d$ – normal stresses induced by characteristic moving load with dynamic coefficient and characteristic dead load [MPa],
- $\sigma_{ao} = \dfrac{0.001M_o}{W_d} + \sigma_{ao,r}$ – normal stresses induced by design load [MPa] with rheological effects taken into consideration ($W_d$ [m$^3$] is bending rate for bottom fibres)

Compression stresses in the top fibres of the RC platform plate [MPa] were calculated according to the formulas [4]:

- $\sigma_{bk} = 0.001(M_{uk} + M_{gk})/\alpha W_g$ – normal stresses induced by characteristic moving load with dynamic coefficient and by characteristic dead load [MPa],
- $\sigma_{bo} = \dfrac{0.001M_o}{\alpha W_g} + \sigma_{bo,r}$ – normal stresses induced by design load [MPa] with rheological effects taken into consideration ($W_g$ [m$^3$] is bending rate for top fibres).

Values of stresses induced by rheological effects $\sigma_{bo,r}$ (concrete creep and shrinkage with creep taken into consideration) were calculated based on the algorithms presented in [4].

According to design rules [3] the ultimate limit state conditions in respect to longitudinal normal stresses take the form

$$\sigma_{ao}(M_o) \le f_{ad},$$
$$\sigma_{bo}(M_o) \le f_{cd}. \tag{2}$$

The limit state condition in respect to deflections has the form

$$w(M_{usk}) \le w_d, \tag{3}$$

where $w_d = L/800$ for $v \le 160$ km/h. The fatigue limit state conditions are in the form

$$\sigma_{ak}(M_{uk}M_{gk}) \le 0.75f_{ad},$$
$$\sigma_{bk}(M_{uk}M_{gk}) \le 0.60f_{ck}. \tag{4}$$

The limit state condition in respect to comfort (imposed on deflections) is in the form

$$w(M_{uk}) \le w_{pd}(L), \tag{5}$$

where $w_{pd}(L) = L/750$ for $v \le 200$ km/h. The limit state condition in respect to rail traffic safety (limitation of deflections under dead load) takes the form

$$w_{\min}(L) \le w(M_{gk}) \le w_{\max}(L) \tag{6}$$

and values $w_{\min}(L)$, $w_{\max}(L)$ are given in [3].

Table 5 collects values of geometric, mass and stiffness parameters of SCB series-of-types bridges, approach slabs and ballasted track, used in numerical modelling of the BTT system. A composite cross-section of a bridge superstructure was reduced to an equivalent steel cross-section. The parameters correspond to Figs. 1–5. Material data given in [1, 2] have been applied. Table 5 includes the following quantities:

- $F(0.5L)$ – area of equivalent cross-section of bridge superstructure, at midspan,
- $h_b(0.5L)$, $h_t(0.5L)$ – vertical distances to bottom and top fibres measured from mass centre of equivalent cross-section of bridge superstructure, at midspan,
- $I(0.5L)$ – geometrical moment of inertia in respect to horizontal central axis of equivalent cross-section of bridge superstructure, at midspan,
- $W_b(0.5L)$, $W_t(0.5L)$ – bending rates for bottom and top fibres of equivalent cross-section of bridge superstructure, at midspan,
- $E = 205$ GPa – Young's modulus of S235W steel (material of main beams),
- $EI(0.5L)$ – flexural stiffness of equivalent cross-section of bridge superstructure, at midspan,
- $m(0.5L)$ – mass per unit length of equivalent cross-section of bridge superstructure, at midspan (with isolation layer, levelling concrete, kerbs, covers, sidewalk, joints, ribs, brackets taken into account),
- $F(0)$, $h_b(0)$, $h_t(0)$, $I(0)$, $W_b(0)$, $W_t(0)$, $EI(0)$, $m(0)$ – geometric, stiffness and mass parameters of equivalent cross-section of bridge superstructure, at support area (without overlay of lower chord of main beams),
- $\gamma$ – Rayleigh damping ratio of bridge superstructure,
- $f_l = 1$ Hz, $f_u = 500$ Hz – vibration frequency range in which damping is approximately constant.

Table 5
Parameters of bridges forming SCB series-of-types

| Parameter | Unit | SCB-15 | SCB-18 | SCB-21 | SCB-24 | SCB-27 |
|---|---|---|---|---|---|---|
| $L$ | m | 15.00 | 18.00 | 21.00 | 24.00 | 27.00 |
| $h_b(0.5L)$ | mm | 735 | 858 | 1009 | 1156 | 1342 |
| $h_t(0.5L)$ | mm | 441 | 518 | 617 | 720 | 834 |
| $I(0.5L)$ | m$^4$ | 0.067789 | 0.101580 | 0.154680 | 0.221439 | 0.311789 |
| $W_b(0.5L)$ | m$^3$ | 0.092242 | 0.118366 | 0.153232 | 0.191603 | 0.232258 |
| $W_t(0.5L)$ | m$^3$ | 0.153681 | 0.196170 | 0.250882 | 0.307435 | 0.374040 |
| $EI(0.5L)$ | Nm$^2$ | $13.897 \times 10^9$ | $20.824 \times 10^9$ | $31.710 \times 10^9$ | $45.395 \times 10^9$ | $63.917 \times 10^9$ |
| $I(0)$ | m$^4$ | 0.050188 | 0.075905 | 0.116859 | 0.168889 | 0.240933 |
| $EI(0)$ | Nm$^2$ | $10.289 \times 10^9$ | $15.561 \times 10^9$ | $23.956 \times 10^9$ | $34.622 \times 10^9$ | $49.391 \times 10^9$ |
| $m(0.5L)$ | kg/m | 5300 | 5470 | 5660 | 5850 | 6020 |
| $m(0)$ | kg/m | 5050 | 5210 | 5380 | 5550 | 5710 |
| $\gamma$ | – | 0.01125 | 0.0075 | 0.005 | 0.005 | 0.005 |

Table 6
Values of bending moments in engineering calculations of bridges forming SCB series-of types

| Parameter | Unit | SCB-15 | SCB-18 | SCB-21 | SCB-24 | SCB-27 |
|---|---|---|---|---|---|---|
| $M_{gk}$ | kNm | 3086.7 | 4353.8 | 6104.6 | 8184.1 | 10439.0 |
| $M_{usk}$ | kNm | 4509.7 | 5981.5 | 7889.6 | 10030.0 | 12243.7 |
| $M_{uk}$ | kNm | 5466.0 | 7035.4 | 9061.8 | 11298.3 | 13568.7 |
| $M_{go}$ | kNm | 4240.3 | 5969.7 | 8352.9 | 11175.6 | 14228.8 |
| $M_{uo}$ | kNm | 8199.0 | 10553.1 | 13592.7 | 16947.5 | 20353.0 |
| $M_o$ | kNm | 12439.3 | 16522.8 | 21945.5 | 28123.1 | 34581.9 |

Table 7
Values of stresses in engineering calculations of bridges forming SCB series-of types

| Parameter | Unit | SCB-15 | SCB-18 | SCB-21 | SCB-24 | SCB-27 |
|---|---|---|---|---|---|---|
| $\sigma_{ao}(M_o)$ | MPa | 134.86 | 139.59 | 143.22 | 146.78 | 148.89 |
| $\sigma_{ao,r}$ | MPa | 5.36 | 5.19 | 5.10 | 5.04 | 5.20 |
| $\sigma_{ao}$ | MPa | 140.22 | 144.78 | 148.32 | 151.82 | 154.09 |
| $f_{ad}$ | MPa | 195 | 195 | 195 | 195 | 195 |
| $\sigma_{bo}(M_o)$ | MPa | 13.66 | 14.22 | 14.76 | 15.44 | 15.60 |
| $\sigma_{bo,r}$ | MPa | $-0.59$ | $-0.74$ | $-0.88$ | $-1.00$ | $-1.12$ |
| $\sigma_{bo}$ | MPa | 13.07 | 13.48 | 13.88 | 14.44 | 14.48 |
| $f_{cd}$ | MPa | 17.5 | 17.5 | 17.5 | 17.5 | 17.5 |
| $\sigma_{ak}(M_{uk}, M_{gk})$ | MPa | 92.72 | 96.22 | 98.98 | 101.68 | 103.37 |
| $0.75f_{ad}$ | MPa | 146.3 | 146.3 | 146.3 | 146.3 | 146.3 |
| $\sigma_{bk}(M_{uk}, M_{gk})$ | MPa | 9.39 | 9.80 | 10.20 | 10.70 | 10.83 |
| $0.60f_{ck}$ | MPa | 15.7 | 15.7 | 15.7 | 15.7 | 15.7 |
| $\sigma_{gk}$ | MPa | 33.47 | 36.78 | 39.84 | 42.71 | 44.95 |

Table 8
Values of deflections in engineering calculations of bridges forming SCB series-of types

| Parameter | Unit | SCB-15 | SCB-18 | SCB-21 | SCB-24 | SCB-27 |
|---|---|---|---|---|---|---|
| $w(M_{usk})$ | mm | 7.9 | 10.1 | 11.9 | 13.8 | 15.1 |
| $w_d$ | mm | 18.8 | 22.5 | 26.3 | 30.0 | 33.8 |
| $w(M_{uk})$ | mm | 9.6 | 11.9 | 13.6 | 15.5 | 16.7 |
| $w_{pd}$ | mm | 20.0 | 24.0 | 28.0 | 32.0 | 36.0 |
| $w(M_{gk})$ | mm | 5.4 | 7.3 | 9.2 | 11.2 | 12.8 |
| $w_{min}$ | mm | 2.2 | 3.0 | 3.5 | 4.0 | 5.0 |
| $w_{max}$ | mm | 10.5 | 17.0 | 20.0 | 22.0 | 25.0 |

Subsequent physical parameters occurring in numerical modelling of BTT systems have the following values [1, 2]: $\rho_b = 2000$ kg/m$^3$ – ballast density, $m_r$, $m_{sr} = 120$ kg/m, $M_r$, $M_{sr} = 72$ kg/m, $M_s = 366$ kg, $m_s = 610$ kg/m, $M_b = 2900$ kg, $m_b = 4833$ kg/m, $m_a = 2000$ kg/m, $L_a = 4.80$ m, $2D = 204$ m where: $m_r$, $M_r$ – mass of main rails per unit length and mass of main rails per one sleeper, $m_{sr}$, $M_{sr}$ – mass of side rails per unit length and mass of side rails per one sleeper, $M_s$, $m_s$ – mass of one sleeper and two fasteners and mass of one sleeper and two fasteners per unit length, $M_b$, $m_b$ – mass of ballast per one sleeper and mass of ballast per unit length, $m_a$ – mass of approach slab per unit length, $L_a$ – length of approach slab, $2D$ – length of out-of-approach zone.

The main results of engineering calculations of bridges forming the SCB series-of-types, with parameters set up in Ta-

ble 5, are given in Tables 6, 7, 8, where $\sigma_{gk} = 0.001 M_{gk}/W_d$ – normal stresses in bottom fibres of main steel beams induced by characteristic dead load [MPa]. Design conditions (2-6) are satisfied.

## 3. Shortened description of mathematical modelling, numerical modelling and simulation of BTT systems

The BTT system has the following inertial subsystems (Figs. 6, 7) [1]: BS – bridge superstructure, LAS – left approach slab, RAS – right approach slab, LB – left ballast-bed, RB – right ballast-bed, SL –sleepers, OR – operating rails, SR –side rails, RV$i$, $i = 1, 2, \ldots, N_v$ – railway vehicles. These subsystems are subject to the relevant subsets of vertical interaction forces, carried by elastic/viscoelastic physically lin-

www.czasopisma.pan.pl    PAN    www.journals.pan.pl
POLSKA AKADEMIA NAUK

*Vertical vibrations of composite bridge/track structure/high-speed train systems. Part 1*

ear/nonlinear constraints. Using Lagrange's equations and the internal assembling, linear matrix equations of motion of individual subsystems with the generalized load vectors stored in an implicit form are obtained. Linear/non-linear interaction forces are transformed into the generalized load vectors. This formulation leads to equations of motion of the subsystems with constant coefficients. Coupling and non-linearity of the subsystems is hidden in the generalized load vectors expressed in terms of the interaction forces. Detailed formulation in reference to mathematical modelling, numerical modelling and simulation of BTT systems is presented in [1, 2]. Symbols marked in Figs. 6–8 are defined in [1]

A 1D physical model of the track structure/bridge subsystem is presented in Fig. 7. A constant sleeper spacing $d$ is used to discretize the subsystem. The main rails are fixed at the ends of the finite-long section of track $4D + L_o$. The side rails are of length of $L_o$ and are rested viscoelastically on the sleepers. Viscoelastic elements modelling the fasteners and the ballast incorporate physically nonlinear elastic constraints. Discretization of beams modelling operating rails, side rails, approach slabs and the bridge superstructure uses finite elements deformed in flexure, with 4DOF and length $d$. Nodes of the finite elements coincide with the positions of the sleepers [1].
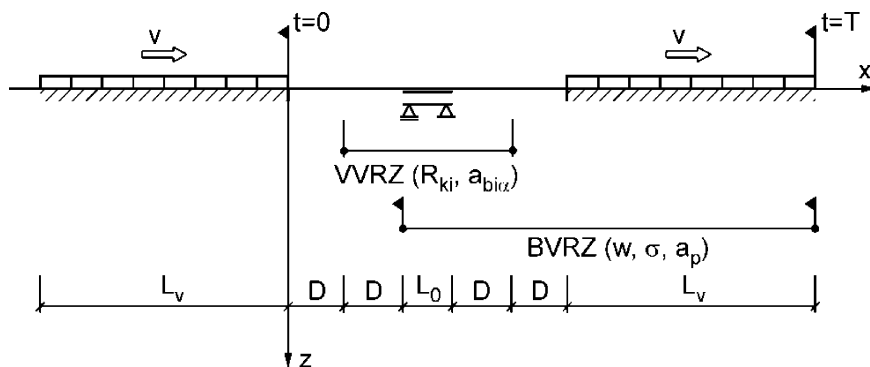


Fig. 6. Schematic diagram of BTT system at time $t = 0$ and $t = T$
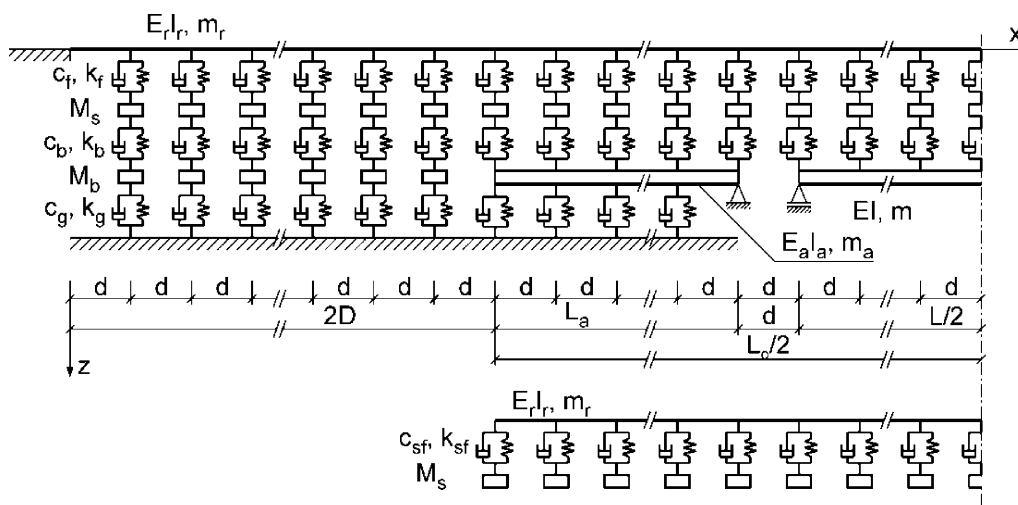


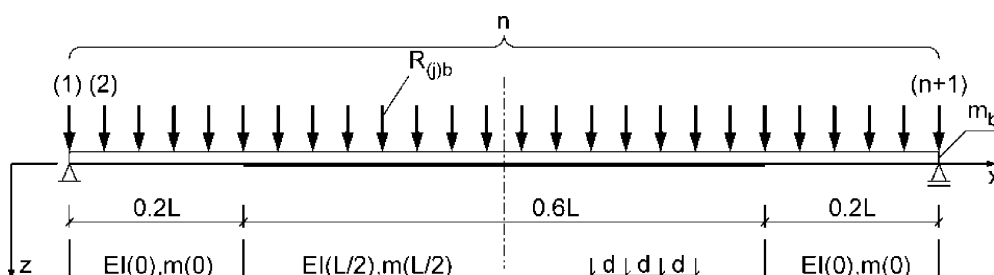Fig. 7. 1D physical model of track structure/bridge subsystem



Fig. 8. 1D physical model of bridge loaded with interaction forces carried by ballast

Ballast mass on the approach slabs and on the bridge is considered in the distributed form. Step-wise changes in the parameters of the bridge superstructure occur in respective nodes of the finite element mesh (Figs. 7, 8) [1]. The physical model of the track/bridge subsystem is symmetrical in reference to the midspan.

Transient and quasi-steady-state vibrations of the BTT system are governed by $8 + N_v$ matrix equations of motion in the following implicit form [1]:

$$\mathbf{B\ddot{q}} + \mathbf{C\dot{q}} + \mathbf{Kq} = \mathbf{F}$$

$$\mathbf{B}_{la}\ddot{\mathbf{q}}_{la} + \mathbf{C}_{la}\dot{\mathbf{q}}_{la} + \mathbf{K}_{la}\mathbf{q}_{la} = \mathbf{F}_{la}$$

$$\mathbf{B}_{ra}\ddot{\mathbf{q}}_{ra} + \mathbf{C}_{ra}\dot{\mathbf{q}}_{ra} + \mathbf{K}_{ra}\mathbf{q}_{ra} = \mathbf{F}_{ra}$$

$$\{\mathbf{M}_b\}\ddot{\mathbf{q}}_{lb} = \mathbf{F}_{lb}$$

$$\{\mathbf{M}_b\}\ddot{\mathbf{q}}_{rb} = \mathbf{F}_{rb} \qquad (7)$$

$$\{\mathbf{M}_s\}\ddot{\mathbf{q}}_s = \mathbf{R}_f - \mathbf{R}_b$$

$$\mathbf{B}_r\ddot{\mathbf{q}}_r + \mathbf{C}_r\dot{\mathbf{q}}_r + \mathbf{K}_r\mathbf{q}_r = \mathbf{F}_r$$

$$\mathbf{B}_{sr}\ddot{\mathbf{q}}_{sr} + \mathbf{C}_{sr}\dot{\mathbf{q}}_{sr} + \mathbf{K}_{sr}\mathbf{q}_{sr} = \mathbf{F}_{sr}$$

$$\mathbf{B}_i\ddot{\mathbf{q}}_i = \mathbf{F}_i, \qquad i = 1, 2, \ldots, N_v$$

where $\mathbf{q}(t)$, $\mathbf{q}_{la}(t)$, $\mathbf{q}_{ra}(t)$, $\mathbf{q}_{lb}(t)$, $\mathbf{q}_{rb}(t)$, $\mathbf{q}_s(t)$, $\mathbf{q}_r(t)$, $\mathbf{q}_{sr}(t)$ – vectors of generalised coordinates for BS, LAS, RAS, LB, RB, SL, OR, SR subsystems, respectively, $\mathbf{q}_i(t)$, $i = 1, 2, \ldots, N_v$ – vectors of generalised coordinates for subsequent rail-vehicles, $\mathbf{B}$, $\mathbf{C}$, $\mathbf{K}$ – mass, damping and stiffness matrices for BS subsystem, respectively, $\mathbf{B}_{la}$, $\mathbf{C}_{la}$, $\mathbf{K}_{la}$, $\mathbf{B}_{ra}$, $\mathbf{C}_{ra}$, $\mathbf{K}_{ra}$ – mass, damping and stiffness matrices for LAS and RAS subsystems, respectively, $\{\mathbf{M}_b\}$ – mass matrix for LB and RB subsystems, $\{\mathbf{M}_s\}$ – mass matrix for SL subsystem, $\mathbf{B}_r$, $\mathbf{C}_r$, $\mathbf{K}_r$, $\mathbf{B}_{sr}$, $\mathbf{C}_{sr}$, $\mathbf{K}_{sr}$ – mass, damping and stiffness matrices for OR and SR subsystems, respectively, $\mathbf{B}_i$ – mass matrix for $i^{th}$ rail-vehicle, $\mathbf{R}_f$, $\mathbf{R}_{sf}$ – vectors of interaction forces transmitted by fasteners in OR and SR subsystems, respectively, $\mathbf{R}_b$ – vector of interaction forces transmitted by ballast-bed, $\mathbf{R}_g$ – vector of interaction forces transmitted by track-bed, $\mathbf{R}_{wi}$ – vector of moving pressure forces of $i^{th}$ vehicle wheel sets acting on rails, $\mathbf{F}(\mathbf{R}_b)$ – generalised load vector in implicit form, related to BS subsystem, $\mathbf{F}_{la}(\mathbf{R}_b, \mathbf{R}_g)$, $\mathbf{F}_{ra}(\mathbf{R}_b, \mathbf{R}_g)$ – generalised load vectors in implicit form, related to LAS and RAS subsystems, respectively, $\mathbf{F}_{lb}(\mathbf{R}_b, \mathbf{R}_g)$, $\mathbf{F}_{rb}(\mathbf{R}_b, \mathbf{R}_g)$ – generalised load vectors in implicit form, related to LB and RB subsystems, respectively, $\mathbf{F}_r(\mathbf{R}_f, \mathbf{R}_{wi})$, $i = 1, 2, \ldots, N_v$, $\mathbf{F}_{sr}(\mathbf{R}_{sf})$ – generalised load vectors in implicit form, related to OR and SR subsystems, respectively, $\mathbf{R}_i = \mathrm{col}(R_{1i} R_{2i} \ldots R_{10,i})$ – vector of vertical interactions transmitted by $1^{st}$ and $2^{nd}$ stage suspensions of $i^{th}$ vehicle, $\mathbf{G}$ – generalised load vector reflecting static pressures of wheel sets onto rails, $\mathbf{F}_i(\mathbf{R}_i, \mathbf{G})$, $i = 1, 2, \ldots, N_v$ – generalised load vector in implicit form, related to RVi, $i = 1, 2, \ldots, N_v$ subsystem, $(\dot{}) = d/dt$ – differentiation with respect to time variable $t$. Detailed formulae defining matrices and vectors in Eq. (7) are given in [1].

Numerical investigations have been carried out for a German passenger train ICE-3. The enhanced Matsuura model of a rail-vehicle equipped with two two-axle bogies is applied. Wheel sets of the vehicle are modelled as point masses vibrating vertically, each with 1DOF. Bogie frames are modelled as rigid disks, each with 2DOF (vertical translation and rotation). The car body is also modelled as a disk with 2DOF. Suspensions of the first and second stage are linear viscoelastic. The masses modelling the wheel sets are fitted with one-sided vertical springs of nonlinear Hertzian contact stiffness reflecting wheel set – rails contact. The detailed description of the rail-vehicle modelling the reader can find in [1].

Based on Eq. (7) and remaining formulae presented in [1], the authors developed a computer programme in Delphi for simulation of dynamic processes in BTT systems.

## 4. Traffic safety and passenger comfort conditions

A dynamic response of a bridge due to a high-speed train is usually described by means of dynamic amplification factors, bridge deck accelerations and vehicle body accelerations. Dynamic amplification factors concern the main output quantities for the bridge superstructure, i.e. the vertical deflection and the longitudinal normal stress in the bottom fibres of the main beams, at the midspan.

Railway bridges loaded by high-speed trains need to be designed or modernized to ensure the traffic safety condition (TSC) and the passenger comfort condition (PCC). UIC (Draft) Code 776-2, "Design requirements for rail bridges based on interaction phenomena between train, track, bridge and in particular speed", Paris, France, Union Int. des Chemins de Fer, 2003 specifies the following conditions [5]:

- the TSC expressed by the limit vertical acceleration of the bridge deck:
  $a_{\mathrm{p,lim}} = 0.35\mathrm{g} = 3.43 \mathrm{\ m/s^2}$,
- the PCC expressed by the limit vertical deflection of the bridge span:
  $w_{\mathrm{lim}} = L/1700$, where $L$ is the bridge span length.

The limits of deformation and vibration to be taken into account for the design of new railway bridges are specified in EN 1990 Eurocode: "Basis of structural design, Annex A2: Application for bridges". Excessive bridge deformations can endanger railway traffic by creating unacceptable changes in vertical and horizontal track geometry and excessive stresses in rails. Excessive vibrations can lead to ballast instability and unacceptable reduction in wheel – rail contact forces. Excessive deformations can also affect the loads imposed on the track/bridge system and create conditions which cause passenger discomfort.

The basic verifications on bridge deformations, performed for TSC condition, are as follows (EN 1990 Eurocode: "Basis of structural design, Annex A2: Application for bridges, EN 1991-2 Eurocode 1: Actions on structures, Part 2: General actions – traffic loads on bridges"):

www.czasopisma.pan.pl  PAN  www.journals.pan.pl
POLSKA AKADEMIA NAUK

*Vertical vibrations of composite bridge/track structure/high-speed train systems. Part 1*

- maximum peak vertical acceleration of the deck due to rail traffic actions (to avoid ballast instability and unacceptable reduction in wheel/rail contact forces),
- vertical deflection of the deck throughout each span (to ensure acceptable vertical track radii and generally robust structures).

The limit value of bridge deck acceleration calculated along the line of a track shall not exceed the design value $a_{p,\lim} = 3.50$ m/s$^2$ for ballasted track. The maximum total vertical deflection of the bridge structure loaded with the classified characteristic vertical loading (not for Real Trains), measured along any track, should not exceed L/600.

Verification on bridge deformations, performed for PCC condition, can be related to vertical deflection of the deck or directly to the carbody vertical acceleration. The indicative levels of comfort, expressed by the vertical acceleration $a_{b,\max}$ inside the carriage during the travel are specified in Table 9 (EN 1990 Eurocode).

Table 9
The indicative levels of passenger comfort

| Level of comfort | $a_{b,\lim}$ [m/s$^2$] |
|---|---|
| very good | 1.0 |
| good | 1.3 |
| acceptable | 2.0 |

## 5. Prediction of forced resonances

The BTT system under consideration is weakly nonlinear physically (ballast, rail fastenings) and maps geometrically infinite track approximately via out-of-approach zones of the track. Based on preliminary simulations, it is concluded that the BT (bridge/track structure) subsystem exhibits modal characteristics similar to those for a linear system. Fundamental modal characteristics of the BT subsystem, called quasi-free damped vibrations, quasinatural frequency can be identified after passage of the high-speed train over the bridge (when the train is in the right out-of-approach zone of the track).

Preliminary calculations identifying the fundamental natural quasi-frequency of the physically nonlinear bridge/track structure subsystem are performed for a selected operating speed, e.g., $v = 250$ km/h. Six last nodes on the chart of quasi-free damped vibrations induced by the passage of the train are identified. Approximate values of the fundamental natural quasi-period and quasi-frequency of the bridge/track subsystem are calculated from the formulae

$$T_1 = \frac{s}{v}, \qquad f_1 = \frac{1}{T_1}, \qquad (8)$$

where $s$ – distance of the load head over one cycle of free damped vibrations (average value corresponding to above noted six last nodes). Periods of subsequent harmonics of the quasi-static excitation of the bridge/track subsystem are

$$\bar{T}_i = \frac{l}{iv}, \qquad i = 1, 2, \ldots. \qquad (9)$$

A prediction of the resonant operating speeds, corresponding to equality of the fundamental natural quasi-period and sub-

sequent harmonics of the quasi-static excitation, is as follows

$$T_1 = \overline{T}_i \Rightarrow T_1 = \frac{l}{iv} \Rightarrow v_{i1} = \frac{l}{iT_1}, i = 1, 2, \ldots, \qquad (10)$$

where the total length of the vehicle equals $l = 24.78$ m.

Due to parametric effects resulting from quasi unsprung moving masses (wheel sets), the more exact resonant operating speeds are lower by $\sim 1.5\%$ compared to the values calculated from Eq. (10). This phenomenon was detected based on preliminary simulations of dynamic processes in BTT systems. Predicted resonant operating speeds decreased by $\sim 1.5\%$ are collected in Table 10.

Table 10
Predicted resonant operating speeds

| Bridge code | $T_1$ [s] | $f_1$ [1/s] | Resonant operating speed [km/h] | | | | |
|---|---|---|---|---|---|---|---|
| | | | $v_{11}$ | $v_{21}$ | $v_{31}$ | $v_{41}$ | $v_{51}$ |
| SCB-15 | 0.163 | 6.14 | 540 | 270 | 180 | 135 | 108 |
| SCB-18 | 0.195 | 5.14 | 450 | 225 | 149 | 112 | 90 |
| SCB-21 | 0.216 | 4.62 | 407 | 203 | 135 | 101 | 82 |
| SCB-24 | 0.238 | 4.20 | 370 | 185 | 123 | 93 | 74 |
| SCB-27 | 0.256 | 3.90 | 343 | 171 | 114 | 86 | 69 |

## 6. Representative results of numerical tests for bridges forming SCB series-of-types

The following output quantities are defined (see Fig. 6):

- $w(0.5Lt)$ – deflection of bridge superstructure at midspan [mm],
- $\sigma(0.5Lt)$ – longitudinal normal stress in bottom fibres of main beams, at midspan [MPa],
- $a_p(0.5Lt)$ – vertical acceleration of RC platform, at midspan [m/s$^2$],
- $R_{1,7}(t)$ – selected dynamic pressure force of wheel set onto rails (1$^{st}$ wheel set of 7$^{th}$ vehicle) [kN],
- $a_{b7f}(t)$ – selected vertical acceleration of carbody (pivot over front bogie of 7$^{th}$ vehicle) [m/s$^2$].

The following design quantities are defined:

$$w_{\max} = \max_t w(0.5L, t) \quad [\text{mm}],$$

$$\sigma_{\max} = \max_t \sigma(0.5L, t) \quad [\text{MPa}],$$

$$a_{p,\max} = \max_t |a_p(0.5L, t)| \quad [\text{m/s}^2],$$

$$R_{\min} = \min_t \{R_{ki}(t), \quad k = 1, 2, 3, 4, \quad i = 1, 2, \ldots, N_v\} \quad [\text{kN}],$$

$$a_{b,\max} = \max_t \{|a_{bi\alpha}(t)|, \quad i = 1, 2, \ldots, N_v, \quad \alpha = fr \quad [\text{m/s}^2],$$
$$(11)$$

where $R_{ki}(t)$, $k = 1, 2, 3, 4$, $i = 1, 2, \ldots, N_v$ – dynamic pressure forces of wheel sets onto rails [kN], $a_{bi\alpha}(t) i = 1, 2, \ldots, N_v$, $\alpha = f, r$ – vertical accelerations of carbodies over front (f) and rear (r) bogie [m/s$^2$].

In reference to the SCB-15 bridge, the simulations were conducted for the ICE-3 train moving at the most dangerous resonant operating velocities, i.e. $v_{31} = 180$ km/h (resonance

of first quasi-modal system with third harmonic component of static periodic moving load), $v_{21} = 270$ km/h (resonance of first quasi-modal system with second harmonic component of the static periodic moving load) and at the maximum operating velocity $v_{max} = 300$ km/h. Analogous simulations were conducted for the remaining bridges forming the SCB type-of-series. Values of the design quantities for bridges SCB-15, SCB-18, SCB-21, SCB-24, SCB-27 are given in Table 11.

The values are compared with those ones for the quasi-static motion of the train ($v = 30$ km/h). Figures 9–13 present time-histories of selected output quantities for the resonant service velocities $v_{31}$ for SCB-15, SCB-18, SCB-21, SCB-24, SCB-27, respectively. Time-histories of dynamic processes are reflected with thin lines ($v = v_{31}$) and are presented against a background of time-histories of quasi-static processes ($v = 30$ km/h) with thick lines.

Table 11
Values of design quantities for bridges forming SCB series-of-types

| Bridge | Operating velocity $v$ [km/h] | $w_{max}$ [mm] | $\sigma_{max}$ [MPa] | $a_{p,max}$ [m/s$^2$] | $R_{min}$ [kN] | $a_{b,max}$ [m/s$^2$] |
|---|---|---|---|---|---|---|
| SCB-15 | $v = 30$ km/h | 2.20 | 13.00 | 0.02 | 156.4 | 0.03 |
| | $v_{21} = 270$ km/h | 5.82 | 38.25 | 6.12 | 136.5 | 0.22 |
| | $v_{31} = 180$ km/h | 6.74 | 43.29 | 7.44 | 141.4 | 0.24 |
| | $v_{max} = 300$ km/h | 4.37 | 27.18 | 3.75 | 138.7 | 0.12 |
| SCB-18 | $v = 30$ km/h | 2.88 | 14.13 | 0.01 | 156.3 | 0.03 |
| | $v_{21} = 225$ km/h | 2.89 | 15.24 | 0.92 | 145.7 | 0.13 |
| | $v_{31} = 149$ km/h | 5.80 | 29.42 | 2.99 | 150.6 | 0.19 |
| | $v_{max} = 300$ km/h | 5.28 | 26.61 | 2.60 | 140.6 | 0.18 |
| SCB-21 | $v = 30$ km/h | 3.22 | 14.01 | 0.01 | 156.3 | 0.02 |
| | $v_{21} = 203$ km/h | 5.38 | 24.32 | 1.94 | 150.4 | 0.21 |
| | $v_{31} = 135$ km/h | 3.79 | 17.17 | 0.78 | 154.6 | 0.11 |
| | $v_{max} = 300$ km/h | 5.87 | 26.00 | 2.59 | 141.4 | 0.19 |
| SCB-24 | $v = 30$ km/h | 3.51 | 13.67 | 0.01 | 156.3 | 0.02 |
| | $v_{21} = 185$ km/h | 6.41 | 25.61 | 2.10 | 151.9 | 0.27 |
| | $v_{31} = 123$ km/h | 6.47 | 25.92 | 2.20 | 149.9 | 0.30 |
| | $v_{max} = 300$ km/h | 7.09 | 27.88 | 2.62 | 143.7 | 0.28 |
| SCB-27 | $v = 30$ km/h | 3.66 | 13.31 | 0.02 | 156.4 | 0.02 |
| | $v_{21} = 171$ km/h | 5.65 | 20.78 | 1.25 | 153.2 | 0.25 |
| | $v_{31} = 114$ km/h | 5.13 | 19.05 | 1.02 | 153.0 | 0.22 |
| | $v_{max} = 300$ km/h | 7.74 | 28.16 | 2.65 | 145.5 | 0.30 |
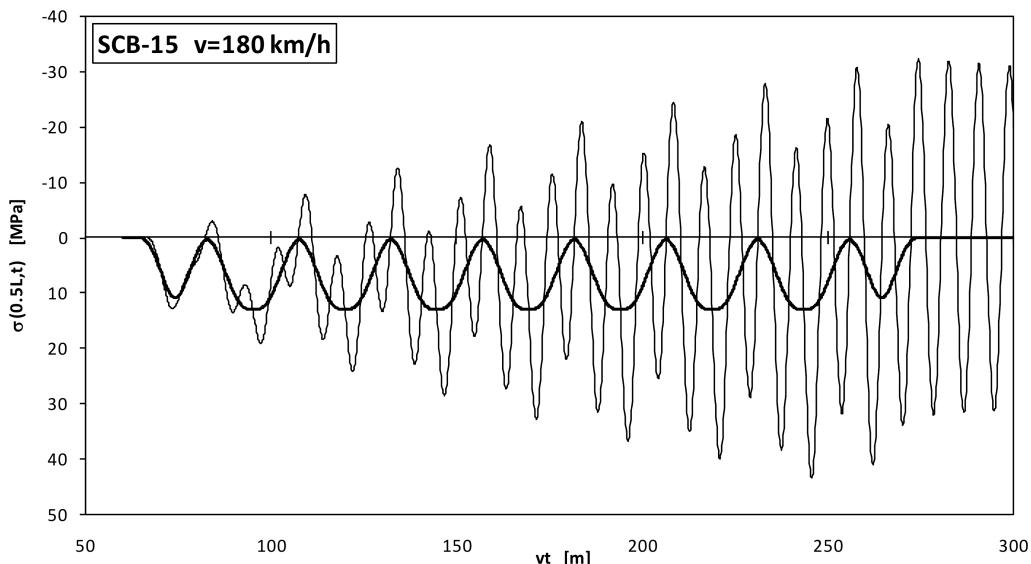


Fig. 9. SCB-15 bridge. Normal stress $\sigma(0.5L, t)$ [MPa] for resonant service velocity $v_{31} = 180$ km/h (thin line) against a background of quasi-static process (thick line)
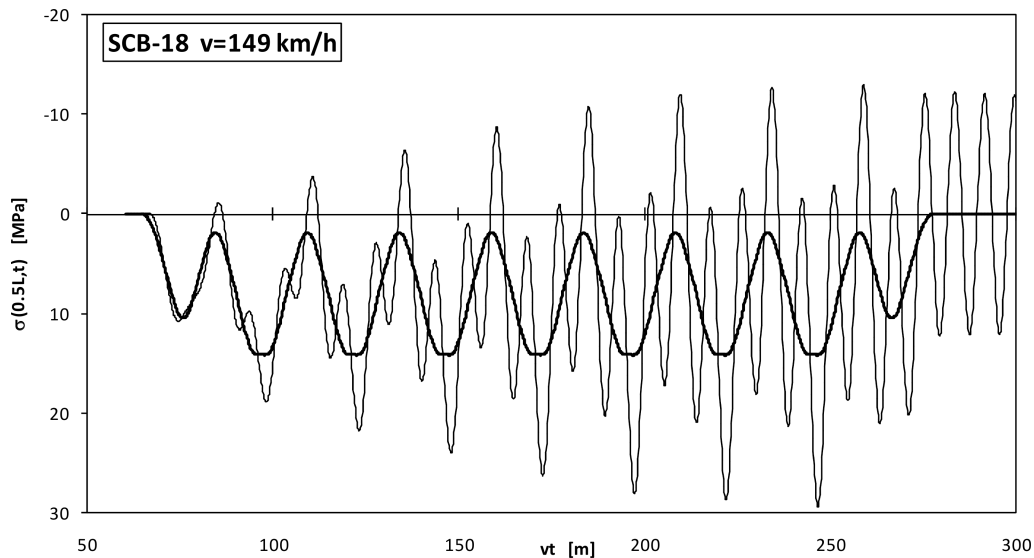
Fig. 10. SCB-18 bridge. Normal stress $\sigma\,(0.5L, t)$ [MPa] for resonant service velocity $v_{31} = 149$ km/h (thin line) against background of quasi-static process (thick line)
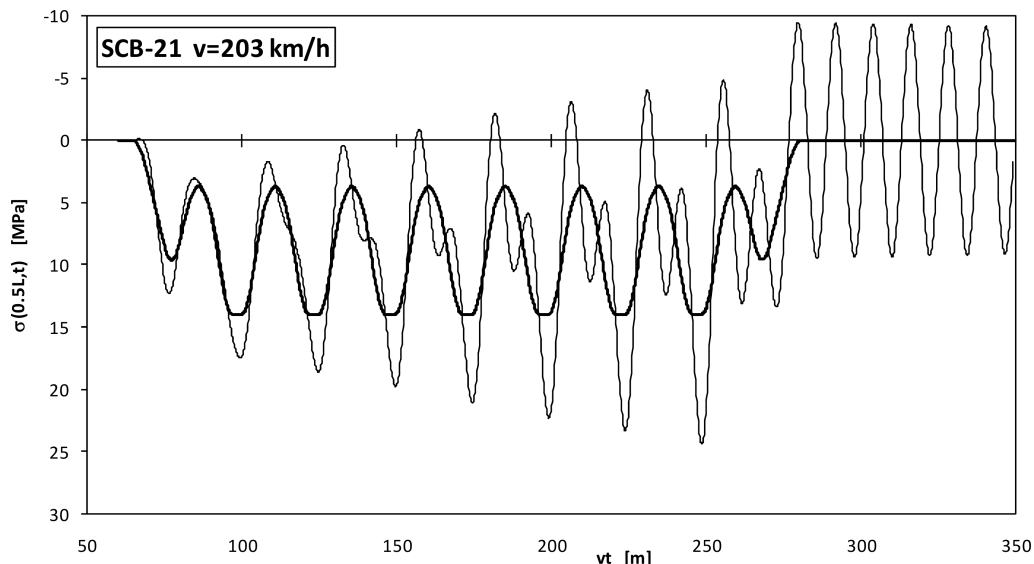


Fig. 11. SCB-21 bridge. Normal stress $\sigma\,(0.5L, t)$ [MPa] for resonant service velocity $v_{31} = 203$ km/h (thin line) against background of quasi-static process (thick line)

Based on Table 11 and Figs. 9–13, the following detailed conclusions are formulated.

1. Values of the dynamic amplification factor in displacement for subsequent bridges, corresponding to an ICE-3 train moving on an even track, differ from each other. At resonant operating velocities, this factor takes the maximum value 3.06 for the shortest bridge SCB-15. At the maximum operating speed, this factor takes the maximum value 2.11 for the longest bridge SCB-27. Some resonant velocities, for SCB-18 and SCB-21 bridges, did not induce resonance amplification effect. The limit state in deflection, expressed by the condition $w_{\max} \leq w_{\lim} = L/1700$, is satisfied for all objects forming the SCB series-of-types, loaded by an ICE-3 high-speed train moving at operating speeds 100–300 km/h.

2. Values of the dynamic amplification factor in stress for subsequent bridges, corresponding to an ICE-3 train moving on an even track, also differ from each other. At resonant operating velocities, this factor takes the maximum value 3.33 for the shortest bridge SCB-15. At the maximum operating speed, this factor takes the maximum value 2.12 for the longest bridge SCB-27. Some resonant velocities, for SCB-18 and SCB-21 bridges, did not induce resonance amplification effect. The fatigue limit state formulated according to [6] is satisfied with safety margin $\sim$1.50 for all objects forming the SCB series-of-types, loaded by an ICE-3 high-speed train moving at operating speeds 100–300 km/h.

3. The limit state of rail traffic safety is satisfied for bridges SCB-18, SCB-21, SCB-24 and SCB-27. For bridge SCB-15 the condition $a_{p,\max} \leq a_{p,\lim} = 3.50$ m/s$^2$ is exceeded about two times at resonant operating speeds and weakly
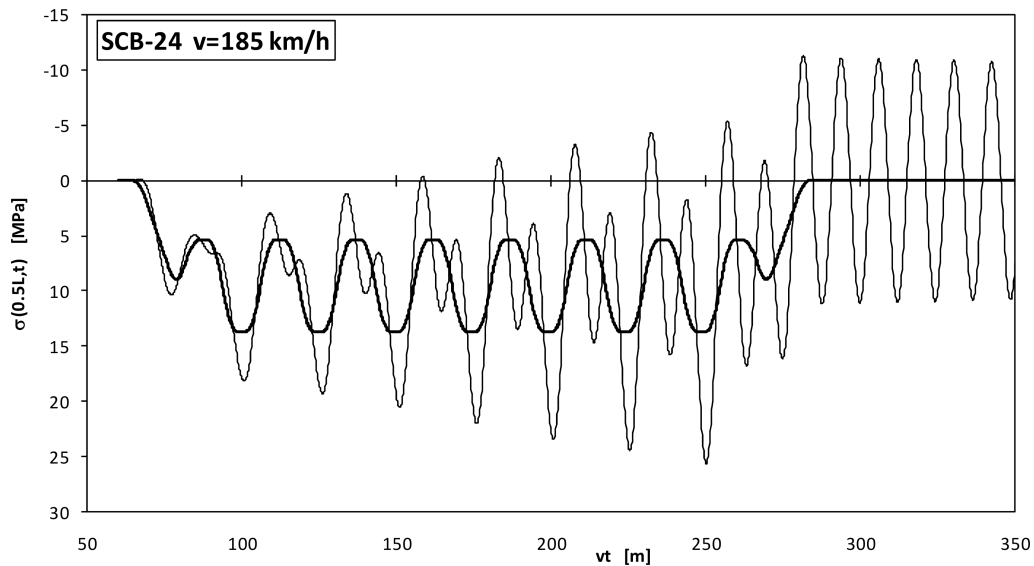
Fig. 12. SCB-24 bridge. Normal stress $\sigma(0.5L, t)$ [MPa] for resonant service velocity $v_{31} = 185$ km/h (thin line) against background of quasi-static process (thick line)
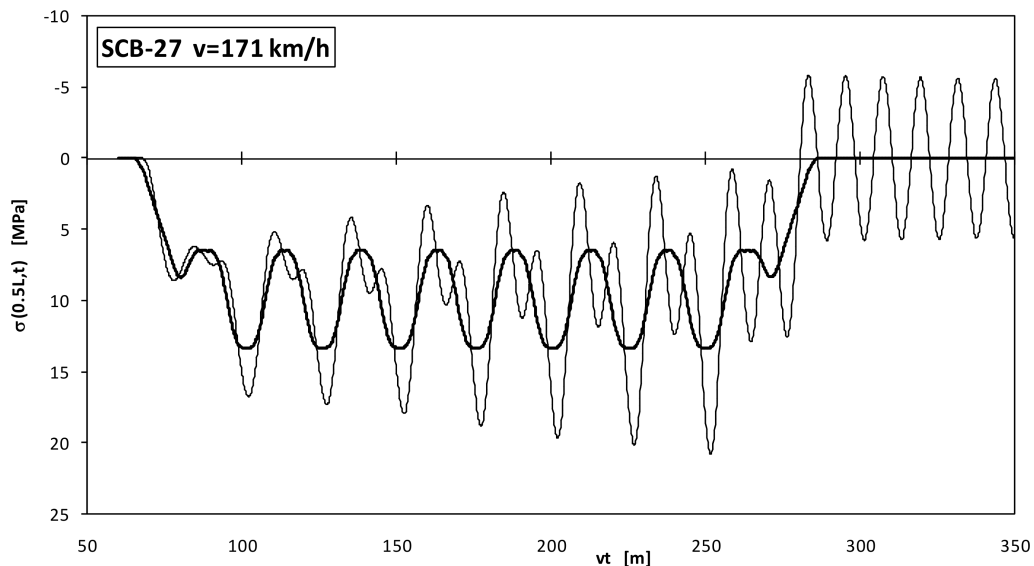


Fig. 13. SCB-27 bridge. Normal stress $\sigma(0.5L, t)$ [MPa] for resonant service velocity $v_{31} = 171$ km/h (thin line) against background of quasi-static process (thick line)

satisfied for the maximum operating speed. Thus, these speeds should be omitted for the shortest bridge span $L = 15$ m.

4. The extreme drop in dynamic pressures of ICE-3 train wheel sets is observed for SCB-15 bridge at the resonant operating speed $v_{21} = 270$ km/h and is equal to 87% of the static pressure force. This drop does not exceed the limit value 75% [6]. Reduction in wheel/rail contact forces is acceptable for all objects forming the SCB series-of-types, loaded by an ICE-3 high-speed train moving at operating speeds 100–300 km/h.

5. The limit state of comfort expressed by the condition $a_{b,max} \leq a_{b,lim}$ is satisfied on a very good level (see Table 9) for all objects forming the SCB series-of-types, loaded by an ICE-3 train moving at operating speeds 100–300 km/h.

## 7. Conclusions

1. The limit state in deflection, expressed by the condition $w_{max} \leq w_{lim} = L/1700$, is satisfied for all objects forming the SCB series-of-types, loaded by an ICE-3 high-speed train moving at operating speeds 100–300 km/h.

2. The fatigue limit state is satisfied with safety margin $\sim$1.50 for all objects forming the SCB series-of-types, loaded by an ICE-3 high-speed train moving at operating speeds 100–300 km/h.

3. The limit state of rail traffic safety is satisfied for bridges SCB-18, SCB-21, SCB-24 and SCB-27. For bridge SCB-15 the condition $a_{p,max} \leq a_{p,lim} = 3.50$ m/s$^2$ is exceeded about two times at resonant operating speeds and weakly satisfied for the maximum operating speed. These speeds should be omitted for the shortest bridge span $L = 15$ m.

4. The extreme drop in dynamic pressures of ICE-3 train wheel sets is observed for SCB-15 bridge at the resonant operating speed $v_{21} = 270$ km/h and is equal to 87% of the static pressure force. This drop does not exceed the limit value 75%. Reduction in wheel/rail contact forces is acceptable for all objects forming the SCB series-of-types, loaded by an ICE-3 high-speed train moving at operating speeds 100–300 km/h.

5. The limit state of comfort expressed by the condition $a_{b,max} \le a_{b,lim}$ is satisfied on a very good level ($a_{b,lim} = 1$ m/s$^2$) for all objects forming the SCB series-of-types, loaded by an ICE-3 high-speed train moving at operating speeds 100–300 km/h.

6. Dynamic phenomena in composite bridge/ballasted track structure/high-speed train systems require experimental investigations focussed on their identification/validation/verification. Such investigations are difficult, time-consuming and expensive; they may be performed by an international research team.

## REFERENCES

[1] M. Podworna and M. Klasztorny, "Vertical vibrations of composite bridge / track structure / high-speed train system. Part 2: Physical and mathematical modelling", *Bull. Pol. Ac.: Tech.* 62 (1), 181–196 (2014).

[2] M. Podworna, M. Klasztorny, "Vertical vibrations of composite bridge / track structure / high-speed train system. Part 3: Deterministic and random vibrations of exemplary system", *Bull. Pol. Ac.: Tech.* 62 (2), (2014), (to be published).

[3] J. Karlikowski, A. Madaj, and W. Wołowicki, *Composite steel – Concrete Bridge Structures*, WKL Press, Warsaw, 2007, (in Polish).

[4] C. Machelski, *Modelling of Bridge Compression*, DWE Press, Wroclaw, 2010, (in Polish).

[5] M.-K. Song, H.-C. Noh, and C.-K. Choi, "A new three dimensional finite element analysis model of high-speed train – bridge interactions", *Engineering Structures* 25, 1611–1626 (2003).

[6] M. Klasztorny, *Dynamics of Beam Bridges under High-speed Trains*, WNT Press, Warsaw, 2005, (in Polish).